Materials Science and Engineering, 56 (1982) 25 - 37

X-ray Residual Stress Measurements on Cold-drawn Steel Wire

P. F. WILLEMSE, B. P. NAUGHTON* and C. A. VERBRAAK

Twente University of Technology, Department of Mechanical Engineering, Materials Section, P.O. Box 217, Enschede (The Netherlands)

(Received October 5, 1981; in revised form February 2, 1982)

SUMMARY

The interplanar spacing $d_{\{hkl\}}$ versus $\sin^2 \psi$ distributions were measured for the 211, 310, 220 and 200 reflections from severely cold-drawn 0.7% C steel wire with a diameter of 0.25 mm. From the shape of the curves it was concluded that, as well as a ⟨110⟩ fibre texture and elastic anisotropy, plastic anisotropy of the ferrite crystals may be an important cause of the non-linearity in $d_{\{hkl\}}$ versus $\sin^2 \psi$. The shape of the curves, and therefore the residual state of stress of the wire, is influenced by the drawing parameters, i.e. the drawing die cone angle and the number of stages.

1. INTRODUCTION

The "$\sin^2 \psi$ technique" is generally used [1] for the measurement of macroscopic residual stresses by means of X-ray diffraction. In this method the interplanar spacing of a given set of planes, $d_{\{hkl\}}$, is measured as a function of $\sin^2 \psi$ where ψ is the angle between the normals to the specimen surface and the reflecting plane. The (residual) stress can then be calculated from the slope of a linear least-squares fit to the measured data and the X-ray elastic constants. In this case a linear relation between $d_{\{hkl\}}$ and $\sin^2 \psi$ is assumed, which can only be expected for a (quasi-)isotropic material. However, non-linear $d_{\{hkl\}}$ *versus* $\sin^2 \psi$ distributions have been reported frequently when materials, after plastic deformation, exhibit both texture and residual stresses [2 - 4]. It is assumed that this non-linearity is primarily due to plastic anisotropy [2], elastic anisotropy [3] or a combination of both [4]. In the present investigation, $d_{\{hkl\}}$ *versus* $\sin^2 \psi$ curves were measured on a cold-drawn steel wire with 0.7% C and a diameter of 0.25 mm. This wire had the normal ⟨110⟩ fibre texture [5]. To investigate the expected effect of the diffraction plane [6, 7], measurements were made on five different reflections: 211, 310, 220, 200 and 222.

2. EXPERIMENTAL PROCEDURE

The measurements were carried out on steel wire with 0.7% C. After the wires had been patented, they were then cold drawn from 1.16 mm to a final nominal diameter of 0.25 mm. The ultimate tensile strength was then about 2650 MPa. Two batches of wire were examined: the wire of batch I was reduced to 0.7 mm diameter in dies with die cone angles 2α of 20° (11 stages) and subsequently with die cone angles of 12° (12 stages); the wire of batch II was reduced entirely in dies with a die cone angle of 12° (16 stages). The final wires were curved (radius of curvature, about 100 mm) because of the coiling. In order to measure $d_{\{hkl\}}$ *versus* $\sin^2 \psi$ curves at certain depths below the original wire surface, the wires were thinned chemically with a solution of 5 parts H_2O, 1 part 70% HF and 14 parts 35% H_2O_2. A ψ goniometer [8, 9] fitted with a proportional counter was used for the X-ray measurements. The collimator of a Philips texture goniometer with an exit 4 mm in width and 0.5 mm in height was used in combination with a point focus and a 0.5° receiving slit. Because the distance from the exit to the specimen was only 30 mm the size of the beam at the specimen was also 4 mm × 0.5 mm.

*Present address: Enka Research Institute, Arnhem, The Netherlands.

0025-5416/82/0000-0000/$02.75

The experimental set-up is shown schematically in Fig. 1(a). The specimens contained 20 - 30 pieces of wire, with a length of 15 mm, which were glued to a Perspex plate (20 mm × 20 mm) with double-stick tape. The plane of curvature (coiling) was parallel to the surface of the Perspex. Figure 1(a) shows the $\psi = 0°, \phi = 0°$ position of the specimen.

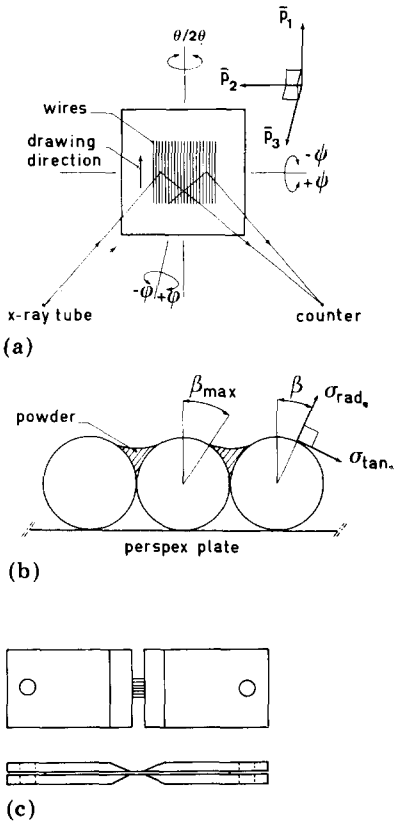

Fig. 1. (a) Relation between the X-ray source, the specimen and the counter (the ψ axis is perpendicular to 2θ–θ as well as to the ϕ axis, and the ϕ axis is perpendicular to the Perspex plate (b); sample system, $\bar{P}_i$; as shown at $\phi = 0°$ and $\psi = 0°$); (b) definition of the tangential stress σ_{tan} and the radial stress σ_{rad} (the axial stress σ_{ax} is perpendicular to σ_{tan}, and σ_{rad} is parallel to the wire axis); (c) the tensile specimen.

It is necessary to screen off part of the wire surface from the primary X-ray beam for the measurements at $\phi = 90°$, as shown in Fig. 1(b). For this purpose, powders with a high absorption coefficient were used. An additional requirement in the choice of these powders is that they do not cause diffraction peaks near to the relevant θ values. For this reason the combinations given in Table 1 were used. In this way the angle β (Fig. 1(b)) could be restricted to a value of about 30°. A graphite monochromator was used with Cu Kα radiation. For the other radiations a β filter and a pulse height analyser were used.

TABLE 1

Combinations of reflections, radiation and powder

Reflection	*Radiation*	*Powder*
211	Co Kα	Pb
310	Co Kα	Sn
220	Fe Kα	Sn
200	Cr Kα	Bismuth oxide
222	Cu Kα	Sn

In addition, tensile specimens as shown in Fig. 1(c) were used for the measurements on unannealed as well as stress-relieved wires which were externally loaded uniaxially. In the latter experiments, 17 pieces of wire were bonded between two copper plates by means of a cyanoacrylate adhesive (Locktite IS 415). For stress relief the wires were annealed at 625 °C for 1 h in vacuum and furnace cooled. The specimen was loaded with the aid of a tensile device mounted on the ϕ axis of the goniometer. The alignment of the ψ goniometer was checked using a flat annealed iron powder specimen and, if necessary, adjusted in such a way that for $+\psi$ and $-\psi$ rotations the position of the diffraction peak was independent of ψ. The position of the specimen with respect to the ψ axis was further adjusted in such a manner that the irradiated surfaces of the wires on both sides of the plane through the ψ axis and perpendicular to the ϕ axis were equal. The peak intensities were measured by means of a step scan procedure with $\Delta(2\theta)$ steps which were chosen between 0.01° and 0.1° depending on the peak width. The maximum of a least-squares quadratic fit for 20 - 30 data above 85% of the maximum net peak intensity was calculated for the determination [10] of the peak position, which was corrected by means of the Rachinger method [11]. Lattice strains were calculated from a comparison with $d_0\{hkl\}$ for the annealed iron powder specimen. "ψ scans" of the {110} planes were measured with a Philips texture goniometer in order to evaluate the fibre texture.

3. RESULTS AND DISCUSSION

3.1. The shape of the $d_{\{hkl\}}$ versus $\sin^2 \psi$ curves

The interplanar spacings $d_{\{211\}}$ as a function of $\sin^2 \psi$ are shown in Fig. 2(a) for wires of batch I in the as-drawn condition and thinned to diameters of 212 and 120 μm. Figure 2(b) shows the corresponding relative maximum peak intensities. The measurements were made for $+\psi$ and $-\psi$ at $\phi = 0°$. A marked systematic difference in $d_{\{211\}}$ *versus* $\sin^2 \psi$ for $+\psi$ and $-\psi$ was not found; therefore the data are averaged for $+\psi$ and $-\psi$. Figure 2(c) shows the results of a ψ scan obtained by diffraction from the {110} planes. The shape of the curve does agree with a ⟨110⟩ fibre texture. The results given in Fig. 2 indicate that the oscillations in the $d_{\{211\}}$ *versus* $\sin^2 \psi$ curves become more pronounced with a sharpening of the ⟨110⟩ texture. The oscillations do not follow the peak intensities as was found by Marion and Cohen [2] for rolled steel. The relations between $d_{\{211\}}$ and $\sin^2 \psi$ for the $\phi = 90°$ position are shown in Fig. 3(a). In this case also, just as for all the measurements mentioned below, no systematic difference for $+\psi$ and $-\psi$ was observed. The values shown are averages for $+\psi$ and $-\psi$. In the $\phi = 90°$ position, $d_{\{211\}}$ *versus* $\sin^2 \psi$ as well as the maximum peak intensity *versus* $\sin^2 \psi$ (Fig. 3(b)) are linear.

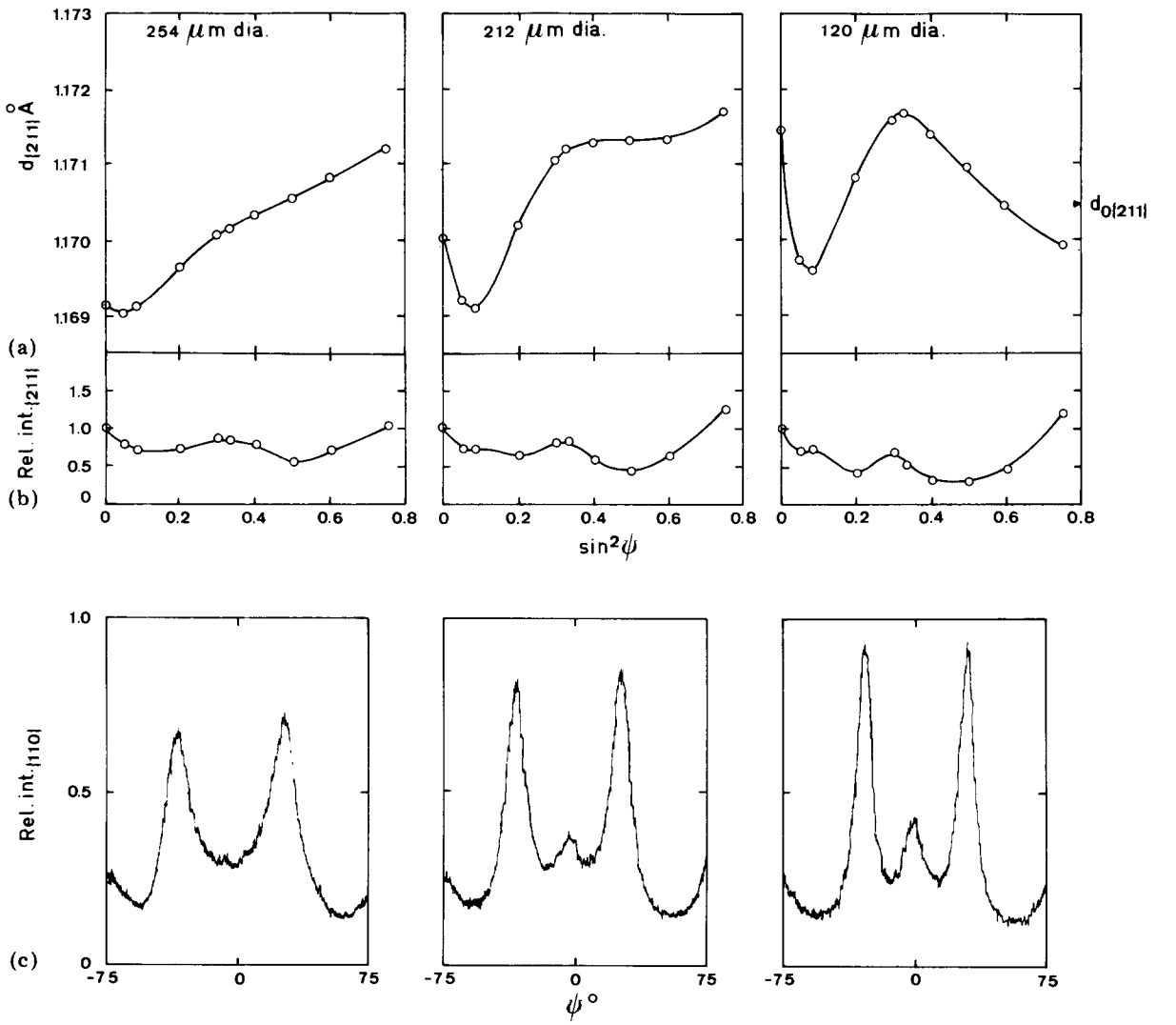

Fig. 2. (a) $d_{\{211\}}$ *vs.* $\sin^2 \psi$ for batch I at $\phi = 0°$ (Co Kα radiation); (b) the relative maximum peak intensity obtained by diffraction from the {211} planes ($\phi = 0°$; Co Kα radiation); (c) results of a ψ scan obtained by diffraction from the {110} planes ($\phi = 0°$; Co Kα radiation).

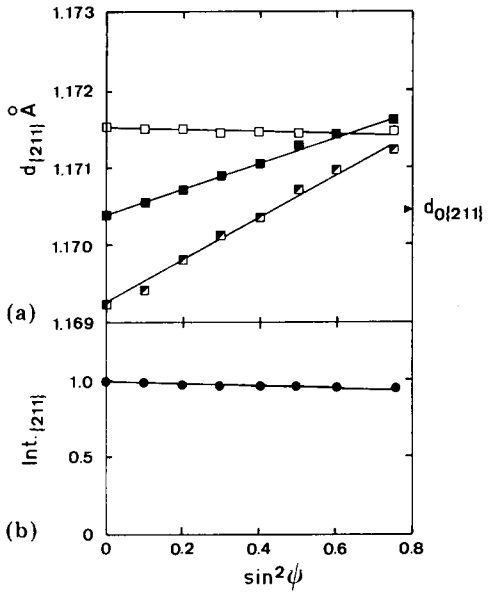

Fig. 3. (a) $d\{_{211}\}$ *vs.* $\sin^2\psi$ for batch I at $\phi = 90°$ (Co Kα radiation) for various diameters (▨, 254 μm; ■, 212 μm; □, 120 μm); (b) the relative maximum peak intensity of the 211 reflections *vs.* $\sin^2\psi$ for specimen I.212 ($\phi = 90°$; Co Kα radiation).

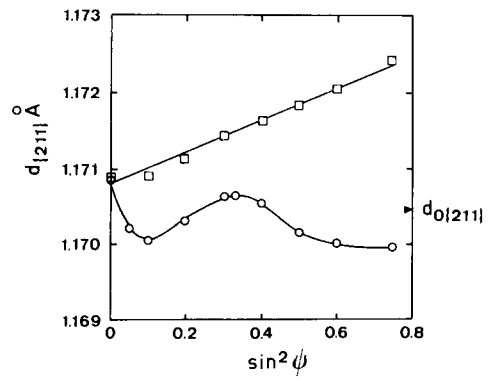

Fig. 4. $d\{_{211}\}$ *vs.* $\sin^2\psi$ for batch II (Co Kα radiation): ○, $\phi = 0°$; □, $\phi = 90°$.

Figure 4 shows $d\{_{211}\}$ as a function of $\sin^2\psi$ for the wires of batch II in the as-drawn condition, for $\phi = 0°$ and $\phi = 90°$.

From a comparison with the results given in Fig. 2(a) (for the unetched wires also) it is obvious that, contrary to the results for batch I, the slope of a linear least-squares fit to the data is now negative. This could indicate that the (pseudo)macrostresses were tensile for batch I and compressive for batch II in an axial direction at the surface. The conclusion that the residual stress is influenced by the drawing parameters, such as the drawing die cone angle and the number of drawing stages, is in agreement with results obtained with mechanical methods on thicker steel wire [12, 13]. The sequence of oscillations, however, is the same in both batches, although the oscillations for batch II are more pronounced. For batch I this shape is different from that expected for an axial tensile stress in a wire with a ⟨110⟩ fibre texture if only the elastic anisotropy is taken into account [14, 15]. The shape of the curve for batch II (which also has a ⟨110⟩ fibre texture) agrees with the elastic anisotropy model for a compressive axial stress.

The problem of the elastic and plastic anisotropy approach was investigated further by measuring the $d\{_{hkl}\}$ *versus* $\sin^2\psi$ curves for 310, 220 and 200 reflections. For this purpose a specimen from batch I etched to a diameter of 212 μm (indicated hereafter as specimen I.212) was used, because the $d\{_{211}\}$ *versus* $\sin^2\psi$ curve for this specimen did not correspond to the elastic anisotropy model.

3.2. *Elastic anisotropy*

The results obtained with specimen I.212 are given in Figs. 5 - 7. The interplanar spacings for the 200 reflection, at $\phi = 0°$, could only be determined at ψ values of 0° and about 45°. The 200 peak intensity at other ψ values was too low for accurate $d\{_{200}\}$ measurements because of the ⟨110⟩ fibre texture. However, from the four values ($\sin^2\psi$ values of 0, 0.4, 0.5 and 0.6) that could be measured it is clear that $d\{_{200}\}$ *versus* $\sin^2\psi$ for $\phi = 0°$ is not linear. This does not support the "elastic anisotropy model" [3, 16] which predicts a linear $\sin^2\psi$ relation for interplanar spacings of the type $\{h00\}$. It is possible that a stress gradient would give some non-linearity [17]. For this reason, wires with an original diameter of 254 μm were etched

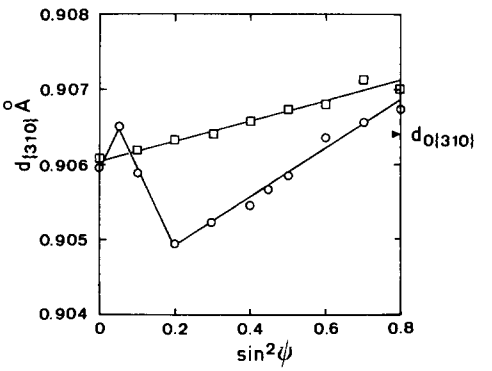

Fig. 5. $d\{_{310}\}$ *vs.* $\sin^2\psi$ for specimen I.212 (Co Kα radiation): ○, $\phi = 0°$; □, $\phi = 90°$.

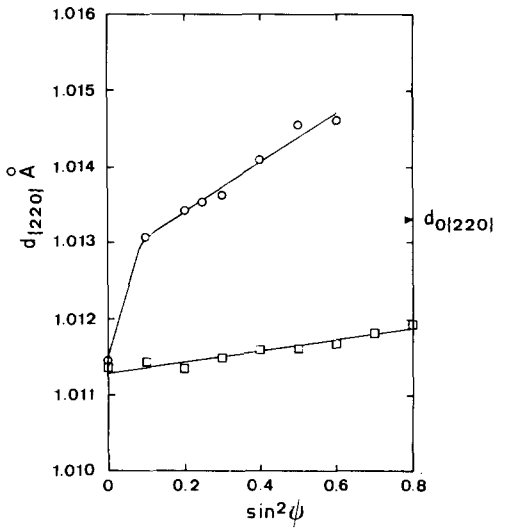

Fig. 6. $d_{\{220\}}$ *vs.* $\sin^2\psi$ for specimen I.212 (Fe Kα radiation): ○, $\phi = 0°$; □, $\phi = 90°$.

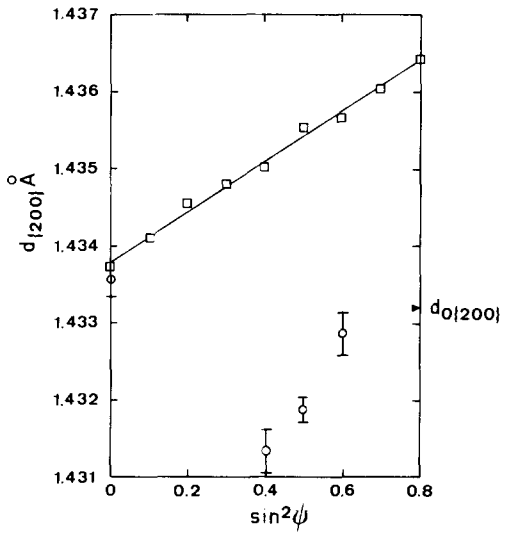

Fig. 7. $d_{\{200\}}$ *vs.* $\sin^2\psi$ for specimen I.212 (Cr Kα radiation): ○, $\phi = 0°$; □, $\phi = 90°$. For $\phi = 0°$ the 90% confidence interval ($n = 6$) is shown.

down to a final diameter of 120 μm in steps 20 μm in diameter (which is equal to 10 μm in surface layer). For each step the $d_{\{211\}}$ *versus* $\sin^2\psi$ curves were measured and the original stress was calculated according to ref. 18 with the "standard" $\sin^2\psi$ method. From these measurements and calculations it could be concluded that no stress gradients larger than 30 MPa μm^{-1} were present. These gradients are insufficient to explain the non-linearity of $d_{\{200\}}$ *versus* $\sin^2\psi$ that is shown in Fig. 7. From the difference between the penetration depth of Cr Kα radiation at $\sin^2\psi = 0.4$ and that at $\sin^2\psi = 0.6$, it could be estimated that a gradient much larger than 200 MPa μm^{-1} would be required to cause the non-linearity shown in this figure. $d_{\{hkl\}}$ *versus* $\sin^2\psi$ at $\phi = 90°$ is linear for the 310, 220 and 200 reflections as it was for the 211 reflection. Although the non-linearity of $d_{\{200\}}$ *versus* $\sin^2\psi$ was not very promising for the elastic anisotropy model [3, 16], a further evaluation of this model was performed with the results of the 211 and 310 reflections.

The principal stresses of an average stress tensor were assumed to be oriented as shown in Fig. 1(b), with the axial stress σ_{ax} perpendicular to the tangential stress σ_{tan} and the radial stress σ_{rad}. This assumption is reasonable because no evidence was found of a systematic difference between $d_{\{211\}}$ *versus* $\sin^2\psi$ at $\phi = 45°$ and the corresponding curve at $\phi = -45°$ nor between $+\psi$ and $-\psi$ at both $\phi = 0°$ and $\phi = 90°$ [19]. A radial stress was included because multi-axial loading during the plastic deformation could possibly produce a pseudomacrostress as a result of the interphase effect due to the approximately 10 vol.% cementite which is present as the second phase [20]. Such a stress could be present in the ferrite and could be balanced by an opposite stress in the very thin lamellae of cementite. First, strains perpendicular to the {211} and {310} planes due to stresses of 1 MPa in an axial, tangential and radial direction were calculated for uncoupled crystallites oriented so as to produce the ideal ⟨110⟩ fibre texture and a uniform stress over the volume (the Reuss limit [21]). For these calculations the equation given by Möller and Martin [22] was used:

$$\begin{aligned}\epsilon_{\phi,\psi} &= \epsilon_{\alpha,\beta,\gamma} \\ &= \sum_{i=1}^{3} \{S_{12} + \\ &\quad + (S_{11} - S_{12})(\alpha^2\eta_i^2 + \beta^2\xi_i^2 + \gamma^2\zeta_i^2) + \\ &\quad + S_{44}(\alpha\beta\eta_i\xi_i + \beta\gamma\xi_i\zeta_i + \alpha\gamma\eta_i\zeta_i)\}\sigma_i \\ &= \sum_{i=1}^{3} F_i^{a}{}_{(\phi,\psi)}\sigma_i \qquad (1)\end{aligned}$$

where ϕ and ψ are defined in Fig. 1(a) ($\phi = 0°$ and $\psi = 0°$ for the wire axis parallel to the θ–2θ axis), α, β and γ are the direction cosines of the normal to the diffracting plane in rela-

tion to the crystal system, η_i, ξ_i and ζ_i are the direction cosines of the principal stresses σ_i in relation to the crystal system ($\sigma_1 = \sigma_{ax}$, $\sigma_2 = \sigma_{tan}$ and $\sigma_3 = \sigma_{rad}$) and $F_i^a{}_{(\phi,\psi)}$ is the anisotropic "compliance". The direction of the measured strain $\epsilon_{\phi,\psi} = (d_{\{hkl\}} - d_{0\{hkl\}})/d_{0\{hkl\}}$ is parallel to the normal to the diffracting plane, *i.e.* to the bisector of the angle between the incident and diffracted X-ray beam. The single-crystal compliances S_{11}, S_{12} and S_{44} for iron were taken from ref. 23. The direction cosines and the ψ values are known because only those lattice planes whose normals are perpendicular to the ψ axis are capable of reflecting (Fig. 8). Consequently the orientation of the corresponding reflecting crystallites can be determined. The fact that the directions of σ_{tan} and σ_{rad} with respect to the reflecting crystallites change because of the cylindrical shape of the wire surface must be taken into account. This was achieved with an integrating procedure with $30° > \beta > -30°$ (Fig. 1(b)).

The values of $\epsilon_{\phi=0°,\psi}/\sigma_i = F^a_{i-(\phi=0°,\psi)}$ are given in Fig. 9 for $\sin^2\psi$ values of 0, 0.08, 0.33 and 0.75 for the 211 reflection and for $\sin^2\psi$ values 0.05, 0.2, 0.45 and 0.8 for the 310 reflection. Figure 9 indicates that the addition of separate strains can lead to various $d_{\{hkl\}}$ *versus* $\sin^2\psi$ distributions, depending

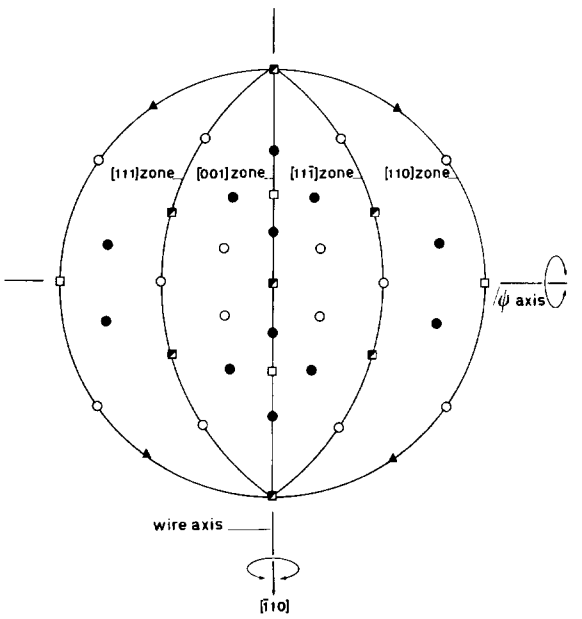

Fig. 8. Stereographic projection with plane normals in relation to the ψ axis for the ϕ = 0° position: □, ⟨100⟩; ▲, ⟨111⟩; ◪, ⟨110⟩; ○, ⟨211⟩; ●, ⟨310⟩.

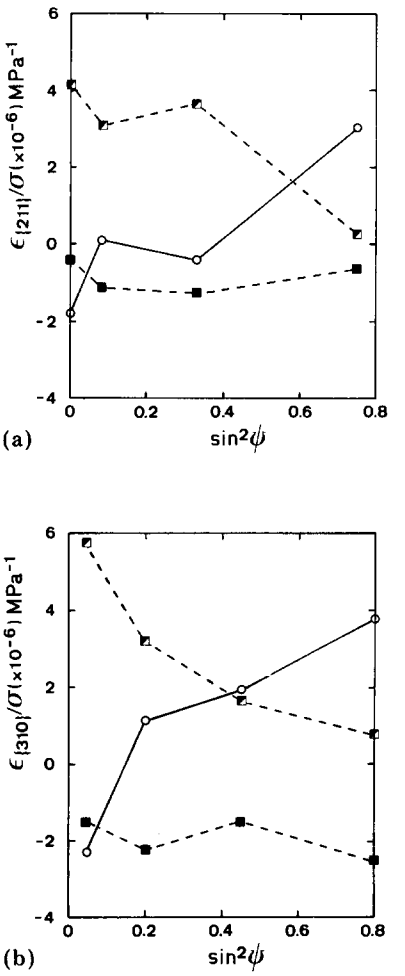

Fig. 9. $\epsilon_{\phi=0°,\psi}/\sigma_i = F_i^a{}_{(\phi=0°,\psi)}$ as a function of $\sin^2\psi$ (wire axis, [1$\bar{1}$0]) for (a) {211} planes and (b) {310} planes: ○, σ_{ax}; ■, σ_{tan}; ◪, σ_{rad}.

on the values and signs of the three principal stresses. In order to calculate the stress tensor from the measured strains, it was assumed, as did Dölle and coworkers [3, 16], that the materials consisted of a volume fraction f^i of grains with a random orientation and a fraction f^a with an orientation corresponding to the ideal ⟨110⟩ fibre texture. According to ref. 16, f^a was estimated from the intensity *versus* $\sin^2\psi$ curve (Fig. 2(b)) to be about $(I_{max} - I_{min})/I_{max} \approx 0.5$. The strains and stresses for the values of $\sin^2\psi$ given in Fig. 9 are related by the "compliances" $F_{i(\phi,\psi)}$ which are a combination of the anisotropic compliances $F_i^a{}_{(\phi,\psi)}$ and the isotropic compliances $F_i^i{}_{(\phi,\psi)}$:

$$F_{i(\phi,\psi)} = f^a F_i^a{}_{(\phi,\psi)} + f^i F_i^i{}_{(\phi,\psi)} \quad (2)$$

The values of $F_i^a{}_{(\phi=0°,\psi)}$ are given in Fig. 9. The isotropic compliances were calculated

from the X-ray elastic constants $S_2/2$ and S_1 for 0.7% C steel given in ref. 24. In the latter case, corrections for the wire geometry had to be made (see Appendix A). The slopes of $d_{\{211\}}$ and $d_{\{310\}}$ *versus* $\sin^2 \psi$ for $\phi = 90°$ were also used (Appendix A), and all strains were averaged for ψ and $-\psi$. Subsequently, "average" ($\sigma_{ax}, \sigma_{tan}$) and ($\sigma_{ax}, \sigma_{tan}, \sigma_{rad}$) stress tensors were calculated from the data, for both the 211 and the 310 reflections (Figs. 2(a), 3(a) and 5), using a least-squares method. However, the calculated interplanar spacings from these tensors did not agree with the measured curves. The differences between the calculated and measured strains had values of up to 100×10^{-5}, and this is much more than the estimated inaccuracy of $(10 - 20) \times 10^{-5}$ for the 211 and 310 reflections. Similar results were obtained for specimens I.254, I.120 and II.255, in this case only for the 211 reflections.

From these results as well as from the fact that $d_{\{200\}}$ *versus* $\sin^2 \psi$ is not linear, it could be concluded that elastic anisotropy is not the main cause of the measured non-linearities. Therefore an examination of the effect of plastic anisotropy was deemed to be necessary.

3.3. *Plastic anisotropy*

In Fig. 10, strains are presented which were calculated from the results given in Figs. 2(a) and 5 - 7 (specimen I.212; $\phi = 0°$), for the directions corresponding to those of an ideal ⟨110⟩ fibre texture. The strains on {222} planes at $\sin^2 \psi = 0.67$ were measured separately with Cu Kα radiation in combination with a graphite monochromator. If [$\bar{1}$10] is taken as the fibre (wire) axis (and the drawing direction), the strains measured on planes which belong to the [001], [11$\bar{1}$], [111] or [110] zone of the anisotropic fraction were selected.

The data from these zones fit straight lines well. This linearity is in accordance with eqn. (1) for the anisotropic case. Appendix A, eqn. (A5), predicts this linearity to a good approximation when the experimental quasi-isotropic X-ray elastic constants for the 211 and 310 reflections [24] and the elastic constants calculated according to Kröner [25] for the 220, 200 and 222 reflections are used. This means that for each group of grains

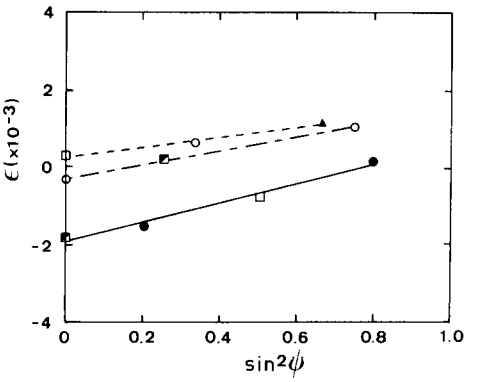

Fig. 10. Residual strains measured on different planes (□, {200}; ▲, {222}; ◩, {220}; ●, {310}; ○, {211}) belonging, for the anisotropic fraction, to the [001] zone (——), the [110] zone (- - - -) and the [11$\bar{1}$] or [111] zones (- — -) (Fig. 8) in grains which are oriented in such a way that these zone axes are parallel to the ψ axis (wire axis, [$\bar{1}$10]; specimen I.212; $\phi = 0°$).

which have their [001], [11$\bar{1}$], [111] or [110] direction parallel to the ψ axis (at $\phi = 0°$), it should be possible to find average stress tensors to fit. These groups will further be referred to as group [001], [11$\bar{1}$], [111] and [110] respectively. The tensors are averaged over the irradiated surface of the wire and the effective penetration depth [8] of the X-rays, which varies from about 1 μm for the 222 reflections at $\sin^2 \psi = 0.67$ to 9 μm for the 310 reflections at $\sin^2 \psi = 0.2$. When a biaxial state of stress is assumed, the principal stresses σ_{ax} and σ_{tan} (Fig. 1(b)) can be calculated by means of eqns. (1) and (A5) from the strains shown in Fig. 10. The calculations were carried out for f^a values of 0.3, 0.5 and 0.7. For the 220, 200 and 222 reflections the isotropic X-ray elastic constants $S_2/2$ and S_1 of iron, calculated according to Kröner's approximation [25], were used in eqn. (A5). The other elastic constants were chosen as mentioned in Section 3.2. The results calculated by a least-squares method are given in Table 2. The estimated error for the stresses due to geometry and counting statistics was about 40 MPa.

It is doubtful, however, whether a biaxial state of stress does exist in this case [17, 26]. For the determination of a triaxial state of stress, strains in additional crystallographic directions which are not perpendicular to the zone axes are needed. These directions must

TABLE 2

Stresses (MPa) calculated for different anisotropic fractions f^a, starting from a biaxial state of stress

Group	$f^a = 0.3$		$f^a = 0.5$		$f^a = 0.7$	
	σ_{ax}	σ_{tan}	σ_{ax}	σ_{tan}	σ_{ax}	σ_{tan}
[001]	565	1105	585	1054	616	1023
[11$\bar{1}$]	270	−168	265	−219	258	−285
[111]	270	−168	265	−219	258	−285
[110]	254	−552	273	−566	292	−582

TABLE 3

Additional directions of the four groups of grains needed to calculate a triaxial state of stress

Group	*Direction*	ϕ (deg)	$\sin^2\psi$ (ψ *positive*)
[001]	[001]	90	1
[110]	[110]	90	1
[11$\bar{1}$]	[00$\bar{1}$]	90	0.33
[11$\bar{1}$]	[$\bar{1}$00]	−39.23	0.83
[11$\bar{1}$]	[0$\bar{1}$0]	−140.77	0.83
[11$\bar{1}$]	[$\bar{1}\bar{1}$0]	−90	0.67
[111]	[00$\bar{1}$]	−90	0.33
[111]	[010]	39.23	0.83
[111]	[100]	140.77	0.83
[111]	[110]	90	0.67

belong to only one of the four groups of grains and are summarized in Table 3.

The additional strains for the [001] and [110] groups cannot be measured because $\sin^2\psi = 1$. These strains were therefore determined by extrapolating $d_{\{220\}}$ and $d_{\{200\}}$ *versus* $\sin^2\psi$ at $\phi = 90°$ to $\sin^2\psi = 1$ (Figs. 6 and 7). It was reasonable to make this extrapolation as $d_{\{hkl\}}$ *versus* $\sin^2\psi$ was found to be linear up to $\sin^2\psi = 0.8$ in both cases.

For groups [11$\bar{1}$] and [111], strains at $\phi = \pm 140.77°$ and $\phi = \pm 39.23°$ were measured separately and did not show a systematic difference; the average strain $\langle\epsilon\rangle$ for these four directions was -70×10^{-5}. The other strains at $\phi = \pm 90°$ could be obtained from Figs. 6 and 7. The following assumptions could be made from considerations of symmetry with respect to the measured strains, the directions of the forces during the plastic deformation process and the orientation of the grains.

(a) For the grains of groups [001] and [110] the principal stresses σ_1, σ_2 and σ_3 coincide with the axes of the orthonormal sample system $\bar{P}_i$ ($\bar{P}_1$ is parallel to the wire axis, $\bar{P}_2$ is perpendicular to the wire axis and parallel to the Perspex plate, and $\bar{P}_3 = \bar{P}_1 \times \bar{P}_2$ (Fig. 1(a))).

(b) The average stress tensor in the grains of groups [11$\bar{1}$] and [111] consists of the components $\sigma_{11}(=\sigma_1)$, σ_{22}, σ_{33}, σ_{23} and σ_{32} with respect to the sample system $\bar{P}_i$.

In order to calculate σ_1, σ_2 and σ_3 for the groups [001] and [110], eqns. (1), (A5) and (A10) were used with $\beta = 0$. To calculate the tensors for groups [11$\bar{1}$] and [111] the equations given by Dölle [17] were applied:

$$\epsilon'_{33} = \epsilon_{\phi,\psi} = R'_{ij}\sigma'_{ij} \tag{3}$$

$$R'_{ij}(hkl, \phi_i, \psi_i) = \frac{f^i r_{ij}(hkl) + f^a S'_{33ij}}{f^i + f^a} \tag{4}$$

$$S'_{33ij} = \lambda_{3m}\lambda_{3n}\lambda_{io}\lambda_{jp}S_{mnop} \tag{5}$$

$$r_{11}(hkl) = r_{22}(hkl) = S_1(hkl) \tag{6a}$$

$$r_{33}(hkl) = S_1(hkl) + \tfrac{1}{2}S_2(hkl) \tag{6b}$$

$$r_{12}(hkl) = r_{13}(hkl) = r_{23}(hkl) = 0 \tag{6c}$$

$$\sigma'_{ij} = \omega_{ik}\omega_{jl}\sigma_{kl} \tag{7}$$

where R'_{ij} are the anisotropic X-ray elastic constants with respect to the orthonormal laboratory system $\bar{L}_i$ ($\bar{L}_3$ and $\bar{L}_2$ coincide with the directions of $\epsilon'_{33} = \epsilon_{\phi,\psi}$ and the ψ axis respectively; $\bar{L}_1 = \bar{L}_2 \times \bar{L}_3$), σ'_{ij} is the stress tensor with respect to $\bar{L}_i$, σ_{kl} is the

TABLE 4

Stresses (MPa) calculated for different anisotropic fractions f^a, starting from a triaxial state of stress

Group	$f^a = 0.3$				$f^a = 0.5$				$f^a = 0.7$			
	σ_1	$\sigma_{2(2)}$	$\sigma_{3(3)}$	σ_{23}/σ_{32}	σ_1	$\sigma_{2(2)}$	$\sigma_{3(3)}$	σ_{23}/σ_{32}	σ_1	$\sigma_{2(2)}$	$\sigma_{3(3)}$	σ_{23}/σ_{32}
[001]	266	442	−184	—	296	433	−183	—	327	423	−187	—
[11$\bar{1}$]	272	−75	−22	228	300	−69	−33	232	331	−65	−46	238
[111]	272	−75	−22	−228	300	−69	−33	−232	331	−65	−46	−238
[110]	350	−194	92	—	361	−212	89	—	374	−231	86	—

stress tensor with respect to $\bar{P}_i$, r_{ij} are the isotropic X-ray elastic constants, f^a and f^i are the anisotropic and isotropic volume fractions respectively, S'_{33ij} are the single-crystal compliances with respect to $\bar{L}_i$, S_{mnop} are the single-crystal compliances with respect to the crystal system, λ is the matrix of the direction cosines between $\bar{L}_i$ and the crystal system and ω is the matrix of the direction cosines between $\bar{P}_i$ and $\bar{L}_i$.

The results of the calculations, for which a least-squares method was again used, are given in Table 4 for f^a values of 0.3, 0.5 and 0.7. The differences between the strains which were calculated from the stress tensors given in Tables 2 and 4 and the measured strains did not exceed the estimated inaccuracy of the measurements. From these results, for all values of f^a considered, the following conclusions can be drawn.

(a) Both for the biaxial and for the triaxial model the tangential directions (σ_{tan} and $\sigma_{2(2)}$) vary strongly from tensile for group [001] to compressive for group [110].

(b) For the triaxial state of stress the radial stress ($\sigma_{3(3)}$) varies also, but in this case from compressive for group [001] to tensile for group [110].

(c) The tangential and radial stresses for group [11$\bar{1}$] and group [111] are relatively low compared with those for the two other groups.

(d) All the calculated stresses in the axial direction are tensile with a relative small variation.

(e) The relatively high values for $\sigma_{3(3)}$, σ_{23} and σ_{32} indicate that the triaxial stress model is more realistic than the biaxial model.

From points (a) and (b) it can be concluded that in both cases the [001] direction is in tension whereas the [110] direction is in compression. This conclusion may be explained in the following way. During the wire drawing, the radial as well as the tangential directions are strained in compression. Young's modulus, the yield stress and the work hardening in a ⟨100⟩ direction have the combined effect that, for a given strain in a ⟨100⟩ direction of a crystal, less stress is required than for the same strain in its surrounding crystals which are differently oriented. After the plastic deformation and elastic spring-back, this would then lead to the intergranular state of stress calculated above [27, 28]. The extent to which the cementite phase and grain boundaries will influence this process remains uncertain. The plastic behaviour of groups [11$\bar{1}$] and [111] may be intermediate between that of group [001] and that of group [110].

For practical applications the following conclusions can be drawn.

(1) Although $d_{\{hkl\}}$ *versus* $\sin^2 \psi$ at $\phi = 90°$ is linear for cold-drawn steel wires, the slope of this plot cannot directly be correlated to the actual stress using the standard $\sin^2 \psi$ method.

(2) However, point (d) shows that the slope of a linear least-squares fit to $d_{\{211\}}$ *versus* $\sin^2 \psi$ at $\phi = 0°$ may give some qualitative information about an axial macrostress. This slope, with $S_2/2 = 5.9 \times 10^{-6}$ MPa^{-1} as determined by a tensile test from $\delta^2 d_{\{211\}}/\delta(\sin^2 \psi)\,\delta\sigma$ [29] yielded a stress of 520 MPa which is, however, higher than the average of the axial microstresses as calculated above but of the same sign.

3.4. Tensile test

Although apparently the elastic anisotropy model is not applicable to plastically deformed wires with a pronounced texture, it should be valid for strains caused by elastic loading. This was investigated on wires of

batch I.212 which were stress relieved by an anneal of 1 h at 625 °C and externally loaded with the aid of a tensile device. After this anneal the ⟨110⟩ fibre texture was retained. For the unloaded specimen, $d_{\{211\}}$ and $d_{\{310\}}$ are linear functions of $\sin^2 \psi$, and $\delta d / \delta(\sin^2 \psi)$ has only a small positive value in both cases (Fig. 11). This linearity confirms that the oscillations observed in the unannealed wires could not have been caused by geometric errors. $d_{\{hkl\}}$ *versus* $\sin^2 \psi$ curves were obtained as also shown in Fig. 11 on loading the wires elastically to an axial tensile stress σ_{ext} of 290 ± 10 MPa. These curves are similar to those given in Fig. 9 for σ_{ax}. Figure 11 also shows the interplanar spacings calculated with the aid of the elastic anisotropy model with $f^a = 0.5$ and $\sigma_{ax} = 290$ MPa. In this calculation, d_0 was derived from the unloaded condition. These calculated values are in good agreement with the experimental

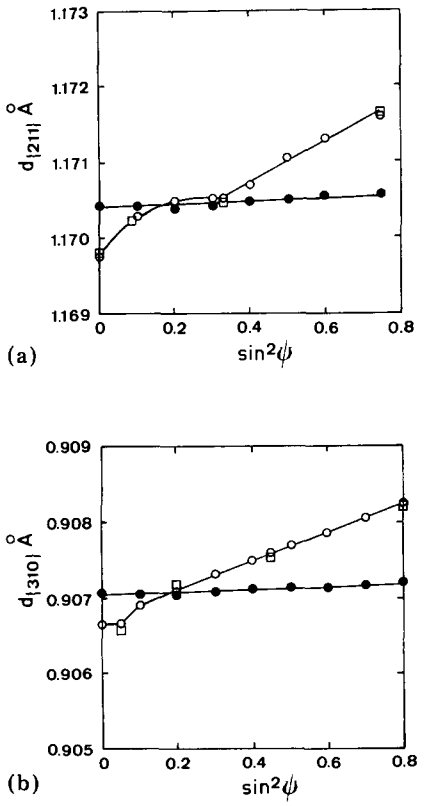

Fig. 11. (a) $d_{\{211\}}$ *vs.* $\sin^2 \psi$ and (b) $d_{\{310\}}$ *vs.* $\sin^2 \psi$ for specimen I.212 after annealing for 1 h at 625 °C, unloaded (●) and loaded (○) to an axial tensile stress σ_{ext} of 290 MPa ($\phi = 0°$; ψ+; Co Kα radiation). Calculated values (□) are also shown.

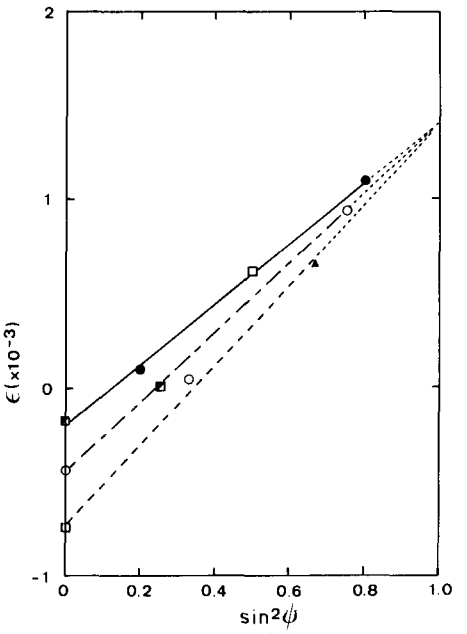

Fig. 12. Strains measured in the same directions as shown in Fig. 10 (the symbols are also as defined in Fig. 10 caption) for the annealed specimen I.212 (1 h at 625 °C) loaded to an axial tensile stress σ_{ext} of 290 MPa ($\phi = 0°$; ψ+).

curves. Furthermore, the $d_{\{hkl\}}$ values for the different zones (similar to Fig. 10) were measured for both the unloaded and the loaded state.

The strains calculated from these d values are shown in Fig. 12. It can be seen that the strains measured on planes which belong to one zone (*i.e.* one group of grains) lie on straight lines, intersecting the same point at $\sin^2 \psi = 1$. From eqn. (1), this point of intersection is expected to occur when the same axial stress is present in each of the four groups of grains mentioned in Section 3.3. σ_{ax} was calculated for the four groups for $f^a = 0.5$ from eqns. (1) and (A5) on the assumption that there is a uniaxial state of stress. The calculated σ_{ax} values for the [001], [110], [111] and [11$\bar{1}$] groups were 298 (±15) MPa, 309 (±15) MPa, 298 (±15) MPa and 298 (±15) MPa respectively. These calculated axial stresses agree well with $\sigma_{ext} = 290 \pm 10$ MPa. From these results it may be concluded that the elastic anisotropy model is applicable to elastically loaded specimens.

4. CONCLUSIONS

From the measurements of $d_{\{hkl\}}$ *versus* $\sin^2 \psi$, where *hkl* is 211, 310, 220 and 200, on cold-drawn 0.7% C steel wire the following conclusions can be drawn.

(1) The shape of the curves, and consequently the state of stress, varies with the drawing die cone angle and the number of drawing stages.

(2) The observed non-linearity in $d_{\{hkl\}}$ *versus* $\sin^2 \psi$ for all reflections, measured in such a position that the ψ axis was perpendicular to the wire axis, could not be explained by a ⟨110⟩ fibre texture and the elastic anisotropy of the grains.

(3) Plastic anisotropy together with the ⟨110⟩ fibre texture seem to be an important cause of the measured non-linearity. Calculation of the average stresses in grains oriented in such a way that their ⟨100⟩, ⟨110⟩ or ⟨111⟩ directions were parallel to the ψ axis showed that a large difference in tangential and possibly radial stresses in these groups of grains may exist.

(4) The $d_{\{hkl\}}$ *versus* $\sin^2 \psi$ relations, measured in a position with the wire axis parallel to the ψ axis, were found to be linear for all reflections. Nevertheless, in terms of the $\sin^2 \psi$ method, the slope of $d_{\{hkl\}}$ *versus* $\sin^2 \psi$ does not give information about the actual state of stress in the separate grains.

(5) The slope of a linear least-squares fit to $d_{\{211\}}$ *versus* $\sin^2 \psi$, measured in a position with the wire axis perpendicular to the ψ axis, gives qualitative information about an axial macrostress.

(6) Strains measured in tensile-loaded wires could be explained in terms of an elastic anisotropy model provided that an anisotropic fraction of grains oriented according to the ideal ⟨110⟩ fibre texture and a fraction of randomly oriented grains are taken into account.

ACKNOWLEDGMENTS

The authors would like to express their thanks to Enka Research Institute, Arnhem, for making the wire-drawing experiments and to Mr. H. Koster for experimental assistance.

REFERENCES

1 E. Macherauch, *Exp. Mech.*, *6* (1966) 140.
2 R. H. Marion and J. B. Cohen, *Adv. X-ray Anal.*, *18* (1975) 446.
3 H. Dölle and V. Hauk, *Z. Metallkd.*, *70* (1979) 682.
4 T. Shiraiwa and Y. Sakamato, *Proc. 13th Jpn. Congr. on Materials Research, Metallic Materials, Kyoto, 1970*, Society for Materials Science of Japan, 1970, p. 25.
5 G. Wassermann and J. Grewen, *Texturen metallischer Werkstoffe*, Springer, Berlin, 1962.
6 F. Bollenrath, V. Hauk and W. Ohly, *Z. Metallkd.*, *57* (1966) 464.
7 N. Hosokawa, K. Honda and J. Arima, *Proc. Int. Conf. on the Mechanical Behaviour of Materials, Kyoto, 1971*, Vol. 1, Society for Materials Science of Japan, 1972, p. 164.
8 U. Wolfstieg, *Härterei-Tech. Mitt.*, *31* (1976) 19.
9 J. Godijk, S. Nannenberg and P. F. Willemse, *J. Appl. Crystallogr.*, *13* (1980) 128.
10 D. Kirk, *Strain*, *7* (1971) 7.
11 W. A. Rachinger, *J. Sci. Instrum.*, *25* (1948) 254.
12 V. J. Zubov, L. A. Krasilnikov and T. N. Krasavina, *Izv. Vysch. Uchebn. Zaved., Chern. Metall.*, *8* (1965) 125.
13 T. Nishisha, *J. Jpn. Inst. Met.*, *20* (1956) 424.
14 V. Hauk and H. Sesemann, *Z. Metallkd.*, *67* (1976) 646.
15 S. Taira and K. Hayashi, *Proc. 13th Japan. Congr. on Materials Research, Metallic Materials, Kyoto, 1970*, Society for Materials Science of Japan, 1970, p. 20.
16 H. Dölle and J. B. Cohen, *Metall. Trans. A*, *11* (1980) 831.
17 H. Dölle, *J. Appl. Crystallogr.*, *12* (1979) 489.
18 M. G. Moore and W. P. Evans, *SAE Trans.*, *66* (1958) 340.
19 V. Hauk, W. K. Krug, G. Vaessen and H. Weisshaupt, *Härterei-Tech. Mitt.*, *35* (1980) 144.
20 D. V. Wilson and Y. A. Konnan, *Acta Metall.*, *12* (1964) 617.
21 A. Reuss, *Z. Angew. Math. Mech.*, *9* (1929) 49.
22 H. Möller and G. Martin, *Mitt. Kaiser-Wilhelm-Inst. Eisenforsch., Düsseldorf*, *21* (1939) 261.
23 *Landolt–Börnstein, New Series*, Group III, Vol. 2, Springer, Berlin, 1969.
24 R. Glocker, *Materialprüfung mit Röntgenstrahlen*, Springer, Berlin, 1971.
25 F. Bollenrath, V. Hauk and E. H. Müller, *Z. Metallkd.*, *58* (1967) 76.
26 K. Nishioka, T. Hanabusa and H. Fujiwara, *Scr. Metall.*, *8* (1974) 1349.
27 G. B. Greenough, *Proc. R. Soc. London, Ser. A*, *167* (1949) 556.
28 G. Fanninger and V. Hauk, *Härterei-Tech. Mitt.*, *31* (1976) 72.
29 V. Hauk and U. Wolfstieg, *Härterei-Tech. Mitt.*, *31* (1976) 38.

APPENDIX A

A.1. Strain–stress relation for the isotropic case

It can be shown that (Fig. A1)

$$\epsilon_{\phi,\psi,\beta} = \epsilon_{ax}\sin^2\psi\cos^2\phi + \epsilon_{tan}(\cos^2\beta\sin^2\phi\sin^2\psi + \sin^2\beta\cos^2\psi - \tfrac{1}{2}\sin 2\beta\sin 2\psi\sin\phi) + \\ + \epsilon_{rad}(\sin^2\beta\sin^2\phi\sin^2\psi + \cos^2\beta\cos^2\psi + \tfrac{1}{2}\sin 2\beta\sin 2\psi\sin\phi) \quad (A1)$$

where ϵ_{ax}, ϵ_{tan} and ϵ_{rad} are the principal strains. The principal strain–principal stress relations, with Young's modulus E and Poisson's ratio ν, are

$$\epsilon_{ax} = \frac{\sigma_{ax}}{E} - \frac{\nu}{E}(\sigma_{tan} + \sigma_{rad}) \quad (A2)$$

$$\epsilon_{tan} = \frac{\sigma_{tan}}{E} - \frac{\nu}{E}(\sigma_{ax} + \sigma_{rad}) \quad (A3)$$

$$\epsilon_{rad} = \frac{\sigma_{rad}}{E} - \frac{\nu}{E}(\sigma_{ax} + \sigma_{tan}) \quad (A4)$$

These are substituted in eqn. (A1). Integration over β between β_{min} and β_{max} (Fig. 1(b), Section 2) gives the average strain over the wire circumference being irradiated. For the $\phi = 0°$ position (ψ axis perpendicular to the wire axis), eqn. (A1) now becomes

$$\langle\epsilon_{\phi=0°,\psi,\beta}\rangle \\ = \{(\tfrac{1}{2}S_2 + S_1)\sigma_{ax} + S_1(\sigma_{tan} + \sigma_{rad})\}\sin^2\psi + \\ + \{(\tfrac{1}{2}S_2 + S_1)\sigma_{tan} + S_1(\sigma_{ax} + \sigma_{rad})\}A\cos^2\psi + \\ + \{(\tfrac{1}{2}S_2 + S_1)\sigma_{rad} + S_1(\sigma_{ax} + \sigma_{tan})\}B\cos^2\psi \quad (A5)$$

with

$$A = \int_{\beta_{min}}^{\beta_{max}} \sin^2\beta\,d\beta \Big/ \int_{\beta_{min}}^{\beta_{max}} d\beta \quad (A6)$$

$$B = \int_{\beta_{min}}^{\beta_{max}} \cos^2\beta\,d\beta \Big/ \int_{\beta_{min}}^{\beta_{max}} d\beta \quad (A7)$$

$$\frac{S_2}{2} = \frac{\nu + 1}{E} \quad (A8)$$

$$S_1 = -\frac{\nu}{E} \quad (A9)$$

where $S_2/2$ and S_1 are the X-ray elastic constants [A1].

For the $\phi = 90°$ position (ψ axis parallel to the wire axis), eqn. (A1) becomes

$$\langle\epsilon_{\phi=90°,\psi,\beta}\rangle \\ = \tfrac{1}{2}S_2(\sigma_{tan} - \sigma_{rad})(C\sin^2\psi - \tfrac{1}{2}D\sin 2\psi + A) + \\ + S_1(\sigma_{ax} + \sigma_{tan}) + (\tfrac{1}{2}S_2 + S_1)\sigma_{rad} \quad (A10)$$

with

$$C = \int_{\beta_{min}}^{\beta_{max}} \cos 2\beta\,d\beta \Big/ \int_{\beta_{min}}^{\beta_{max}} d\beta \quad (A11)$$

$$D = \int_{\beta_{min}}^{\beta_{max}} \sin 2\beta\,d\beta \Big/ \int_{\beta_{min}}^{\beta_{max}} d\beta \quad (A12)$$

A is defined by eqn. (A6), and $D = 0$ for $|\beta_{min}| = |\beta_{max}|$. Differentiation of eqn. (A10) now results in

$$\frac{\partial(\langle\epsilon_{\phi=90°,\psi,\beta}\rangle)}{\partial(\sin^2\psi)} = \tfrac{1}{2}S_2(\sigma_{tan} - \sigma_{rad})C \quad (A13)$$

It is assumed that every part of the wire surface that is irradiated (between β_{min} and β_{max}) contributes equally to the measured diffraction peak intensity. Equation (A13) was used to work out the $d_{\{310\}}$ and $d_{\{211\}}$ *versus* $\sin^2\psi$ curves at $\phi = 90°$ (Section 3.2). In this case the experimental quasi-isotropic

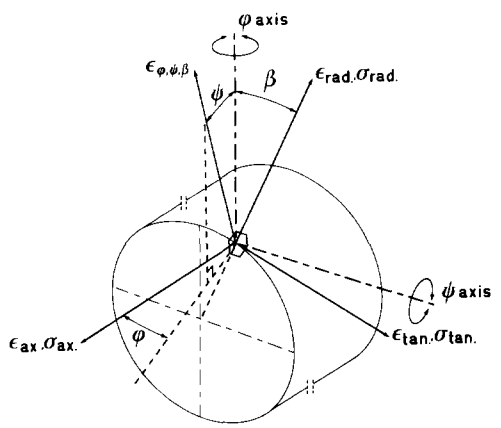

Fig. A1. Strain–stress situation for the isotropic case.

X-ray elastic constant for the 310 reflection from the literature [A1] was applied ($S_2/2 = 7.48 \times 10^{-6}$ MPa^{-1}). For the 211 reflection, $S_2/2$ was taken as a weight average of the experimental quasi-isotropic value [A1] ($S_2/2 = 6.35 \times 10^{-6}$ MPa^{-1}) and an anisotropic value $S_2^a/2$ which was calculated from the single-crystal elastic constants of iron [A2]. For this purpose, $\epsilon_{\phi=90°,\psi}/\sigma_{\tan,\beta=0°}$ was calculated from eqn. (1) for seven different crystallographic directions perpendicular to the wire (fibre) axis ([$\bar{1}$10]) and, consequently, seven different values of ψ. The quotient is nearly a linear function of $\sin^2 \psi$ (correlation coefficient $r = 0.985$) and from the slope of a linear least-squares plot it follows that

$$\frac{\partial \epsilon_{\phi=90°,\psi}/\sigma_{\tan,\beta=0°}}{\partial(\sin^2 \psi)} = \frac{S_2^a}{2}$$

$$= 7.30 \times 10^{-6} \text{ MPa}^{-1}$$

REFERENCES FOR APPENDIX A

A1 R. Glocker, *Materialprüfung mit Röntgenstrahlen*, Springer, Berlin, 1971.

A2 *Landolt–Börnstein, New Series*, Group III, Vol. 2, Springer, Berlin, 1969.